

## Formative evaluation and structural analysis of non-tuberculosis mycobacterial biofilm using material pieces

Kentaro Yamamoto<sup>a,\*</sup>, Shota Torigoe<sup>a,b</sup>, Hirotaka Kobayashi<sup>c</sup>

<sup>a</sup> Department of Mycobacteriology, Leprosy Research Center, National Institute of Infectious Diseases, Aoba-cho, Higashimurayama, Tokyo, Japan

<sup>b</sup> Research Center for Biosafety, Laboratory Animal, and Pathogen Bank, National Institute of Infectious Diseases, Toyama, Shinjuku-ku, Tokyo, Japan

<sup>c</sup> Department of Pathology, National Institute of Infectious Diseases, Toyama, Shinjuku-ku, Tokyo, Japan

### ARTICLE INFO

#### Keywords:

Non-tuberculosis mycobacteria  
Biofilm  
Medical material  
Ultrastructure

### ABSTRACT

Non-tuberculosis mycobacteria (NTM) can form biofilms on diverse artificial surfaces. In the present study, we induced NTM biofilm formation on materials used in various medical devices, evaluated the total amount of biofilm, and observed the ultrastructure by scanning electron microscopy.

### Main text

Biofilms are complex structures formed by the matrix-like entanglement of extracellular secretory components of bacteria, environmental substances, cell bodies, and others. It is known that biofilms have various components, including polysaccharides, proteins, lipids, nucleic acids, and dead bacteria. The properties and structures of biofilms depend on the bacterial species and growth environment (Flemming & Wingender, 2010). Biofilms function as a barrier to protect the bacteria from toxic substances in the exterior environment, antimicrobial agents, chemical disinfectants, and the host defense, serving as the interior like a bacterial shelter (Davies, 2003). In recent years, a significant issue has emerged in the medical field: intractable bacterial infections, specifically biofilm infections resulting from the formation of biofilms on indwelling medical devices such as catheters and artificial joints (Khattoon et al., 2018). Among biofilm infections, especially non-tuberculosis mycobacteria (NTM), which are potentially resistant to various antimicrobial agents and chemical disinfectants, causes more severe disease and possible difficulty to treat (Munoz-Egea et al., 2023, Yamamoto et al., 2023). There have been reported cases in which NTM biofilms formed on catheters, causing severe bacteremia. Furthermore, a global outbreak was caused by the contamination with NTM biofilm at the manufacturer of the heat cooling system for artificial heart-lungs used in cardiac surgery (El Helou et al., 2013, Schreiber et al., 2021). However, NTM biofilms have been studied for a single or very limited area of materials where biofilms form, and comprehensive analyses have not

been conducted under various environments yet. In this study, we demonstrated how biofilms of varying structures are formed by NTM species on different material pieces and in various areas of the materials. We also observed the ultrastructure of each biofilm at different formation areas by scanning whole material pieces using a Field Emission Scanning Electron Microscope (FE-SEM). The three NTMs used in the experiment were *Mycobacterium avium*, *M. intracellulare*, and *M. abscessus*, which are mostly responsible for causing NTM disease (Ratnatunga et al., 2020). The materials were selected mainly from those most frequently used as medical devices: polypropylene (PP), acrylic (Ac), silicon (Si), glass (GL), titanium (Ti), and steel use stainless 304 (SUS). Mycobacterial biofilms tend to form thickly at the air-liquid interface. However, for a more comprehensive understanding of NTM biofilms, it is important to understand not only the interface but also the biofilm structure formed at the point where it is immersed in the culture medium (Intermediate area) and at the point of contacting the bacteria and metabolites accumulated at the bottom of the wells (Tip). Therefore, in this study, we established the dimensions of the material pieces as 10 × 21 × 2 mm (width × length × thickness). We attached these pieces of material to a TestPiece Holder and performed biofilm formation experiments (Fig. 1a).

To facilitate the formation of NTM biofilms on vertical pieces of material, 7H9 medium without tween-80 is required to be supplemented with a reducing agent, Dithiothreitol (DTT), and NTMs need to be incubated under microaerobic conditions and cultivated in a slight water stream. As a result, most biofilms were formed around the

\* Corresponding author.

E-mail address: [keyam@niid.go.jp](mailto:keyam@niid.go.jp) (K. Yamamoto).

<https://doi.org/10.1016/j.tcs.2024.100125>

Received 18 March 2024; Received in revised form 6 May 2024; Accepted 13 May 2024

Available online 14 May 2024

2468-2330/© 2024 The Author(s). Published by Elsevier B.V. This is an open access article under the CC BY-NC-ND license (<http://creativecommons.org/licenses/by-nc-nd/4.0/>).

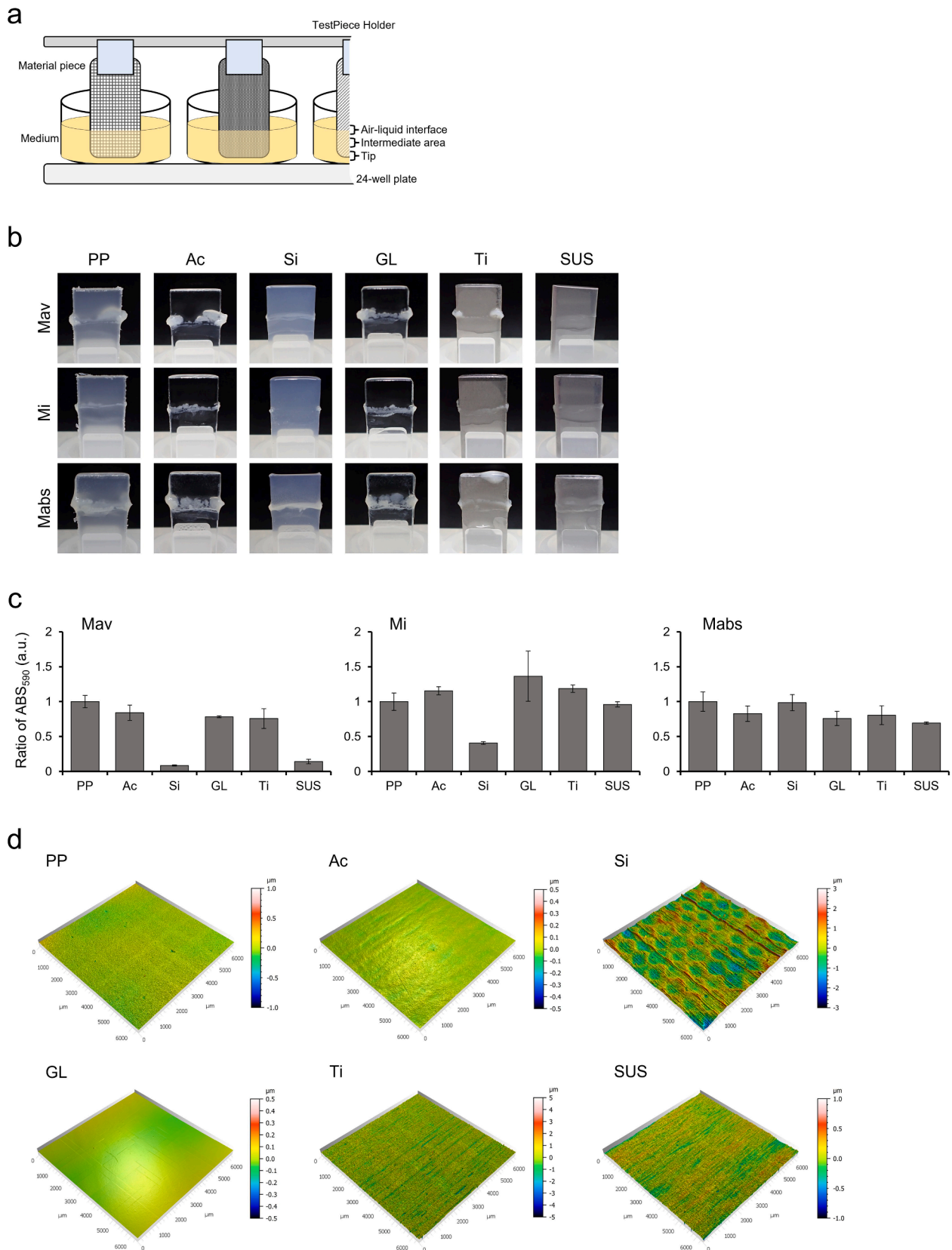


**Fig. 1. Comparison of biofilm formation ability on material pieces.** Biofilms of *M. avium* (Mav), *M. intracellulare* (Mi), and *M. abscessus* (Mabs) were formed on each material piece. (a) The material pieces were suspended in the TestPiece Holder to allow the formation of biofilm on each piece. (b) Macroscopic images of each NTM biofilm on a material piece were presented. (c) The absorbance value of the dye extracted from stained biofilm on PP was used as a baseline, against which the absorbance values of biofilms on other materials were compared. (d) The surface structure of the material pieces was visualized using 3D white light interference microscopy.

air-liquid interface area in all combinations of NTM species and materials (Fig. 1b). This is also consistent with previous reports (Totani et al., 2017). In some combinations, we also observed visual biofilm formation in the intermediate and at the tip areas of the material pieces. For the evaluation of biofilm formation, we stained the samples with crystal violet and measured the absorbance of the extracts of the dye after washing (Fig. 1c). The measurement showed that *M. avium* formed less biofilm on Si and SUS than the other materials. *M. intracellulare* also formed less biofilm on Si, but the biofilm formed on SUS was comparable to that on PP, whereas they formed more biofilm on GL than on PP. Both *M. avium* and *M. intracellulare* are NTMs classified as *Mycobacterium-avium-complex* (MAC), but clinically, MAC disease caused by *M. intracellulare* has a more rapid disease progression and worse prognosis (Koh et al., 2012). Although NTM biofilm infections originating from prosthetics do not often identify the species, the fact that even the same MAC species have different tendencies to form biofilms is considered clinically important. *M. abscessus* formed similar levels of biofilm on all tested materials. In particular, *M. abscessus* formed numerous biofilms even on Si, a surface on which biofilms were not formed easily by the two species of MAC bacteria. Although it should be considered that *M. abscessus* grows more rapidly than MAC species, an important aspect in understanding NTM biofilm infection diseases is that *M. abscessus*, which is potentially one of the most drug-resistant mycobacteria, can easily form biofilms on various materials even under the same culture conditions (Lee et al., 2015). On the other hand, when focusing on the surface roughness of the material pieces, GL had the smoothest surface, and Si had the most undulating and remarkably rough surface (Fig. 1d). However, there was no clear correlation between the surface roughness of the material pieces and the amount of biofilm formation. It has been reported that the adhesion of bacterial cells to substrates is influenced by various factors, including the surface roughness, surface charge, surface tension, and ion distribution of the substrate; thus, it would require a physicochemical approach to investigate the details of the adhesive force between the substrate material and the bacilli (Achinah et al., 2019).

Next, we fixed the biofilm on the material piece set in the TestPiece Holder and observed the ultrastructure by FE-SEM (Fig. 2). As a result, biofilms were formed with each characteristic structure by combinations of the bacterial species and each material piece. In particular, interesting structures were observed in the biofilms formed by *M. avium* on GL and SUS, characterized by overflowing bacilli from smooth, sheet-like membrane with virtually no gaps (Fig. 2, asterisks). Dokic et al. reported that *M. abscessus* forms thick, membrane-like structures that could be considered extracellular matrix (ECM), within which pores and channels were observed (Dokic et al., 2021). It has also been reported that pathogenic bacteria *Leptospira interrogans* form biofilms on a glass surface, which closely resemble the sheet-like structures produced by *M. avium* at the air-liquid interface (Ristow et al., 2008). It is assumed that the space beneath these sheet-like structures, including pore-like formations, plays a crucial role in supplying nutrients and oxygen to the bacteria embedded within. The total amount of biofilm also tended to be greater when the biofilm contained such structures. The biofilms formed on Si by *M. avium* and *M. intracellulare* contained almost no special structure and there was minimal or simple bacterial adhesion. The biofilm of *M. abscessus* also had no unique ultrastructure on Si; however, we observed many bacterial accumulations at the air-liquid interface and in the intermediate area. Specifically, we observed many granular components among *M. abscessus* bacteria at the interface of all materials, suggesting that these components could strengthen the bonds among the *M. abscessus* bacilli (Fig. 2, arrowheads). Lemassu et al. reported that rapidly growing mycobacteria such as *M. smegmatis* and *M. phlei* tend to contain more protein than carbohydrate in their ECM, and it is suggested that the granular structure often observed in the ECM produced by *M. abscessus* might primarily be composed of protein (Lemassu et al., 1996, Dokic et al., 2021). Further studies, including component analysis of each biofilm, are necessary to clarify this

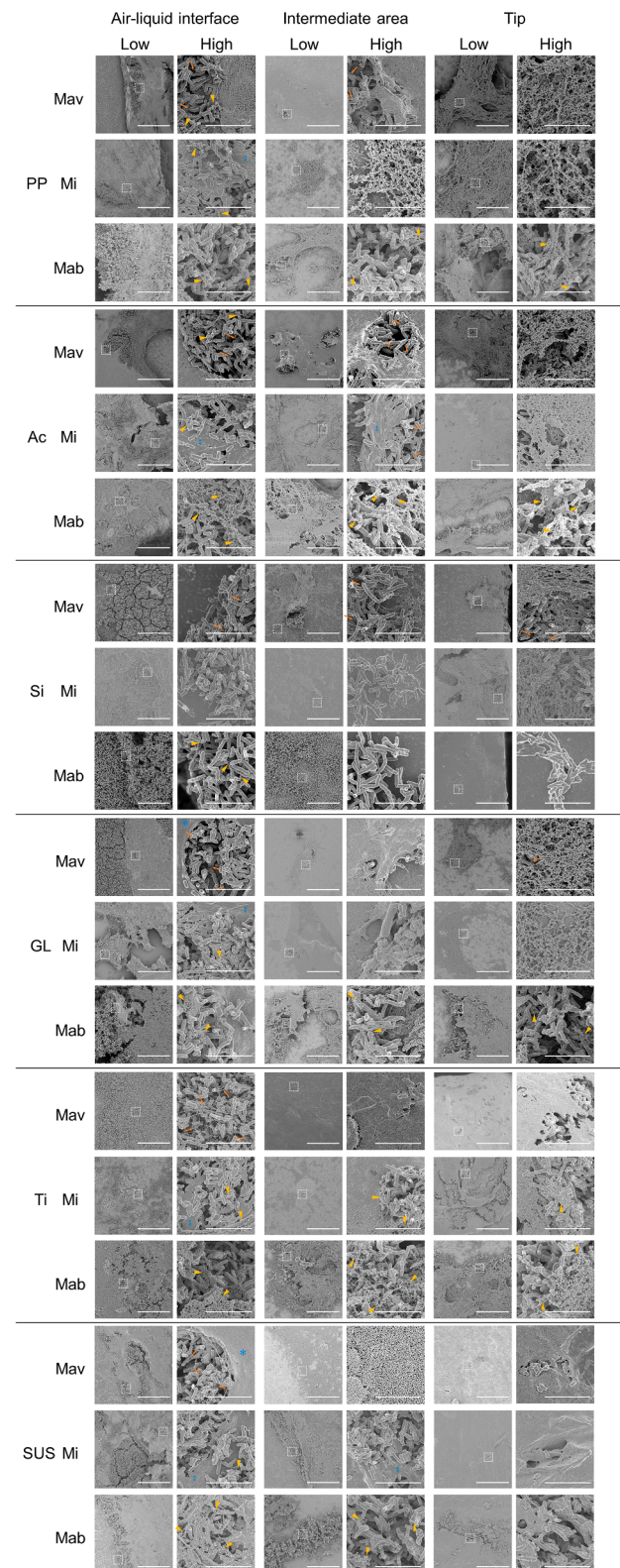


**Fig. 2. Ultrastructures of the biofilm formed on each material piece surface.** These structures were observed in three regions using FE-SEM. Each area enclosed by a white square was observed under high magnification. Each scale bar represents 50 μm at low magnification (Low) and 5 μm at high magnification (High). Arrowheads indicate granular structures observed between bacterial cells; arrows indicate fibrous structures; asterisks indicate thick, gapless sheet-like membrane structures; and double-asterisks indicate thin, smooth sheet-like structures.

possibility. Although the amount and structure of interfacial biofilms on SUS did not show significant difference among the three NTM species, *M. avium* had less biofilm formation and bacterial adhesion in the intermediate areas and at the tips of the material pieces compared to the other two species. This difference appears to be reflected in the difference in total biofilm amount by crystal violet staining. Siddam *et al.* reported that *M. chimaera*, with a slow growth rate, had less tendency to form biofilms on silicon surfaces than on metal surfaces. In contrast, *M. fortuitum*, with a fast growth rate, formed biofilms on silicon surfaces as easily as or more easily than on metal surfaces (Siddam *et al.*, 2020). It is consistent with the material preference for biofilm formation of MAC bacteria and *M. abscessus* in this experiment, so there may be some correlation between the growth rate of NTMs and the property and structure of the bacterial or biofilm surface. On the other hand, most of the material pieces lacked the sheet-like biofilm structures in the intermediate area that were present in the air–liquid interface area. However, it was observed that in many cases, granular or fibrous components formed a matrix structure in which the bacteria accumulated. The granular structure seemed to attach earlier to the substrate surface, which could be the origin of the bacterial attachment to the substrate. The combination with a larger amount of total biofilm tended to show greater bacterial accumulation in the liquid area. In the tip area, granular components predominantly accumulated, but these structures did not often mix with the large number of bacteria. It is possible that this was caused by physical inhibition of bacterial attachment due to frequent exposure to dead bacteria, secreted components of bacteria, medium components, and other debris that had accumulated at the bottom of the wells. Focusing on the connections among the cells in the biofilm, *M. avium* appeared to possess fibrous components linking between cells to strengthen their adhesion. We frequently observed this fiber-like structure, especially in the metallic materials Ti and SUS (Fig. 2, arrows). Since granular component fills the intercellular spaces in the biofilm of *M. abscessus*, and this component was rich in the tips of the material pieces to which the other two species of NTM were rarely attached, it might be a necessary structure for *M. abscessus* to form a strong biofilm. Though *M. intracellulare* biofilms contained few fibers and granules, we observed a thin, smooth sheet-like structure covering the top of the accumulated bacteria (Fig. 2 double-asterisks). Fibrous ECM components have been observed in a variety of bacterial biofilms and are believed to help bind the ECM and cells together, as well as enhance the biofilm's rigidity (Dragos *et al.*, 2017; Barran-Berdon *et al.*, 2020). It has been reported that amyloid fibers are critical for the function of quorum sensing, a bacterial signaling system, in biofilms formed by *Pseudomonas aeruginosa* (Seviour *et al.*, 2015). Additionally, mycobacteria secrete significant quantities of cellulose during the biofilm formation, both in vitro and in vivo. The fibrous structure shown in Fig. 2 closely resembles the SEM image of cellulose microfibrils produced by *M. tuberculosis*, suggesting that cellulose is a crucial component of the biofilm structure in mycobacteria (Trivedi *et al.*, 2016). Indeed, these biofilms can be degraded by exposure to cellulases (Chakraborty *et al.*, 2021; Yamamoto *et al.*, 2023).

In conclusion, these findings reveal that the combination of only three types of mycobacteria and six types of materials can significantly influence the amount of biofilm formation and its structure. Accordingly, when studying mycobacterial biofilms, it is necessary to consider the materials and areas that form the biofilms as well as the species of bacteria and culture conditions. These insights are expected to contribute to the fundamental analysis of NTM biofilms and the development of new medical device materials to prevent biofilm formation.

In this experiment, NTM biofilms were formed as follows. *Mycobacterium avium* subsp. *hominissuis*, *M. intracellulare* subsp. *intracellulare* (ATCC 13950), and *M. abscessus* subsp. *abscessus* (ATCC 19977) were grown to reach their late logarithmic growth phase in 7H9 medium (Middlebrook 7H9 medium supplemented with 0.2% glycerol and 10% OADC) without Tween-80, and cells were then diluted to OD = 0.2 with the above medium. DL – dithiothreitol was added to this bacterial

solution at a final concentration of 6 mM. The material was cut into pieces of 10 × 21 × 2 mm (width × length × thickness) (Standard Test Piece, Inc.), cleaned with 70% ethanol, and sterilized under UV for 20 min. The sterilized pieces were attached to a TestPiece Holder (Dojindo Laboratories Co., Ltd., Tokyo, Japan) and immersed in the adjusted bacterial solution seeded on a 24-well plate (Corning Inc., NY, USA). Samples were cultured at 37°C in an 8% O<sub>2</sub> atmosphere (MITSUBISHI GAS CHEMICAL COMPANY, INC., Tokyo, Japan) using rotational culture (110 rpm) for nine days. Biofilms formed on the material pieces were stained with a 0.1% crystal violet solution (MilliporeSigma, MA., USA) in PBS for 20 min, prewashed with PBS-submerged incubation for 5 min, and immersed in 80% ethanol for 10 min to extract the dye. The extracted dye's absorbance (590 nm) was measured using a multimode microplate reader (Nivo 3S; PerkinElmer, MA, USA). The 3D roughness of the material pieces was visualized using a 3D white light interference microscopy (Opt-scope R200, Tokyo Seimitu Co., Ltd., Tokyo, Japan) with a × 10 objective lens at a pitch of 1.08 μm. Biofilms were ultrastructurally analyzed by FE-SEM as follows. Biofilms were fixed with 2.5% glutaraldehyde and 2% paraformaldehyde in PBS overnight at 4°C, dehydrated in a graded ethanol series (50%–100%) at room temperature, and dried in a critical point dryer using CO<sub>2</sub> (CPD300, Leica Microsystems, Wetzlar, Germany). The samples were then coated with osmium using an osmium plasma coater (Neoc-Pro/P, Meiwafofosis, Tokyo, Japan) and finally visualized with FE-SEM (SU8600, Hitachi High-Tech, Tokyo, Japan) at an accelerating voltage of 1 kV.

#### CRedit authorship contribution statement

**Kentaro Yamamoto:** Writing – review & editing, Writing – original draft, Visualization, Validation, Supervision, Software, Resources, Project administration, Methodology, Investigation, Funding acquisition, Formal analysis, Data curation, Conceptualization. **Shota Torigoe:** Writing – review & editing, Writing – original draft, Methodology, Investigation, Data curation. **Hirotaka Kobayashi:** Writing – review & editing, Writing – original draft, Visualization, Methodology, Investigation.

#### Declaration of competing interest

The authors declare the following financial interests/personal relationships which may be considered as potential competing interests: Kentaro Yamamoto reports financial support was provided by The Ministry of Education, Culture, Sports, Science and Technology (MEXT). If there are other authors, they declare that they have no known competing financial interests or personal relationships that could have appeared to influence the work reported in this paper.

#### Acknowledgments

We thank Drs. Y. Miyamoto, Y. Maeda, Y. Tsujimura and M. Ato for their supports. This work was supported partly by MEXT KAKENHI Grant Number 23K14524, partly by AMED under Grant Number 23fk0108673. The authors would like to thank Enago (www.enago.jp) for the English language review.

#### Author contributions statement

K. Y. participated in the overall study design and analyzed all results, and performed the bacterial preparations for biofilm formation, the staining and analysis of biofilm, and wrote the manuscript. S. T. also designed the experiments and performed preliminary experiments for the biofilm formation and wrote the manuscript. H. K. performed the ultrastructure imaging of biofilm using FE-SEM.

## References

- Achinas, S., Charalampogiannis, N., Euverink, G.J.W., 2019. A brief recap of microbial adhesion and biofilms. *Appl. Sci.* 9, 2801.
- Barran-Berdon, A.L., Ocampo, S., Haider, M., et al., 2020. Enhanced purification coupled with biophysical analyses shows cross-beta structure as a core building block for *Streptococcus mutans* functional amyloids. *Sci. Rep.* 10, 5138.
- Chakraborty, P., Bajeli, S., Kaushal, D., Radotra, B.D., Kumar, A., 2021. Biofilm formation in the lung contributes to virulence and drug tolerance of *Mycobacterium tuberculosis*. *Nat. Commun.* 12.
- Davies, D., 2003. Understanding biofilm resistance to antibacterial agents. *Nat. Rev. Drug Discov.* 2, 114–122.
- Dokic, A., Peterson, E., Arrieta-Ortiz, M.L., Pan, M., Di Maio, A., Baliga, N., Bhatt, A., 2021. *Mycobacterium abscessus* biofilms produce an extracellular matrix and have a distinct mycolic acid profile. *Cell Surf.* 7, 100051.
- Dragos, A., Kovacs, A.T., Claessen, D., 2017. The role of functional amyloids in multicellular growth and development of gram-positive bacteria. *Biomolecules* 7.
- El Helou, G., Viola, G.M., Hachem, R., Han, X.Y., Raad, I.I., 2013. Rapidly growing mycobacterial bloodstream infections. *Lancet Infect. Dis.* 13, 166–174.
- Flemming, H.C., Wingender, J., 2010. The biofilm matrix. *Nat. Rev. Microbiol.* 8, 623–633.
- Khatoun, Z., McTiernan, C.D., Suuronen, E.J., Mah, T.F., Alarcon, E.I., 2018. Bacterial biofilm formation on implantable devices and approaches to its treatment and prevention. *Heliyon* 4, e01067.
- Koh, W.J., Jeong, B.H., Jeon, K., Lee, N.Y., Lee, K.S., Woo, S.Y., Shin, S.J., Kwon, O.J., 2012. Clinical significance of the differentiation between *Mycobacterium avium* and *Mycobacterium intracellulare* in *M. avium* complex lung disease. *Chest* 142, 1482–1488.
- Lee, M.R., Sheng, W.H., Hung, C.C., Yu, C.J., Lee, L.N., Hsueh, P.R., 2015. *Mycobacterium abscessus* complex infections in humans. *Emerg. Infect. Dis.* 21, 1638–1646.
- Lemassu, A., Ortalo-Magne, A., Bardou, F., Silve, G., Laneelle, M.A., Daffe, M., 1996. Extracellular and surface-exposed polysaccharides of non-tuberculous mycobacteria. *Microbiology (Reading)* 142 (Pt 6), 1513–1520.
- Munoz-Egea, M.C., Akir, A., Esteban, J., 2023. Mycobacterium biofilms. *Biofilm* 5, 100107.
- Ratnatunga, C.N., Lutzky, V.P., Kupz, A., Doolan, D.L., Reid, D.W., Field, M., Bell, S.C., Thomson, R.M., Miles, J.J., 2020. The rise of non-tuberculosis mycobacterial lung disease. *Front. Immunol.* 11, 303.
- Ristow, P., Bourhy, P., Kerneis, S., Schmitt, C., Prevost, M.C., Lilenbaum, W., Picardeau, M., 2008. Biofilm formation by saprophytic and pathogenic leptospires. *Microbiology (Reading)* 154, 1309–1317.
- Schreiber, P.W., Kohl, T.A., Kuster, S.P., Niemann, S., Sax, H., 2021. The global outbreak of *Mycobacterium chimaera* infections in cardiac surgery—a systematic review of whole-genome sequencing studies and joint analysis. *Clin. Microbiol. Infect.* 27, 1613–1620.
- Seviour, T., Hansen, S.H., Yang, L., et al., 2015. Functional amyloids keep quorum-sensing molecules in check. *J. Biol. Chem.* 290, 6457–6469.
- Siddam, A.D., Zaslav, S.J., Wang, Y., Phillips, K.S., Silverman, M.D., Regan, P.M., Amarasinghe, J.J., 2020. Characterization of biofilm formation by *Mycobacterium chimaera* on medical device materials. *Front. Microbiol.* 11, 586657.
- Totani, T., Nishiuchi, Y., Tateishi, Y., Yoshida, Y., Kitanaka, H., Niki, M., Kaneko, Y., Matsumoto, S., 2017. Effects of nutritional and ambient oxygen condition on biofilm formation in *Mycobacterium avium* subsp. *hominissuis* via altered glycolipid expression. *Sci. Rep.* 7, 41775.
- Trivedi, A., Mavi, P.S., Bhatt, D., Kumar, A., 2016. Thiol reductive stress induces cellulose-anchored biofilm formation in *Mycobacterium tuberculosis*. *Nat. Commun.* 7, 11392.
- Yamamoto, K., Tsujimura, Y., Ato, M., 2023. Catheter-associated *Mycobacterium intracellulare* biofilm infection in C3HeB/FeJ mice. *Sci. Rep.* 13.